ACS APPLIED NANO MATERIALS

www.acsanm.org Article

Two-Dimensional Silver-Metalated Graphdiyne Nanosheets for Photocatalytic Degradation of Antibiotics

Runhao Huang,[#] Zhenhui Kou,[#] Raul D. Rodriguez, Xusheng Wang, Yang Hou, Tao Wang,* and Tao Zhang*

Cite This: *ACS Appl. Nano Mater.* 2023, 6, 7395−7403 Read Online

ACCESS | Metrics & More | Article Recommendations | Supporting Information

ABSTRACT: The two-dimensional layered carbon allotrope graphdiyne (GDY) is formed by combining hybridized sp−sp^2 carbon atoms. This alkynyl-bonded 2D carbon network with tunable energy levels and high carrier-mobility has excellent potential in solar energy utilization. However, the standard but complex synthesis method of GDYs by epitaxial growth on a metal-crystal surface and the poor activity of metal-free materials limit applications beyond the lab. Here, we produce a silver-metalated GDY (Ag-GDY) through a facile and scalable wet-chemistry strategy, featured by an appropriate band gap at 2.61 eV and good e^-/h^+ separation ability. These unique characteristics facilitate the reaction between Ag-GDY and oxygen to form a variety of active free radicals. The Ag-GDY photocatalyst displays an excellent ability for the light-driven decomposition of antibiotics. Tetracycline with a concentration as low as 5.0×10^{-5} M is degraded within 30 min by Ag-GDY, showing excellent performance stability of up to five reuse cycles.

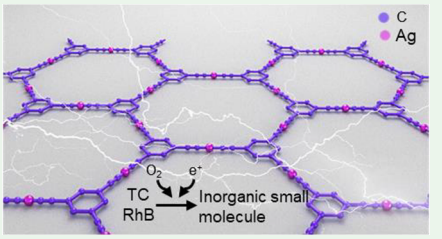

KEYWORDS: *2D carbon material, metalated graphdiyne, interfacial polymerization, photocatalysis pollutant degradation, photoelectrochemistry*

1. INTRODUCTION

Graphdiyne (GDY),[1,2] as a new 2D carbon material with a highly conjugated network mainly composed of sp and sp^2 hybrid carbon atoms, has great potential in photo-[3,4] and electro-catalysis,[5] owing to its unique structural and photoelectric characteristics including: (i) a high surface area and well-distributed pore-structure;[6] (ii) an intrinsic band gap, high carrier mobility, and rapid electrons and holes migration;[7] and (iii) large π-conjugated structure and favorable charge-transfer ability.[1] Especially, like other carbon materials (such as graphene, C_3N_4, etc.), the catalytic performance of GDY can also be tuned by introducing heteroatoms and functional groups.[8] This functionalization allows optimizing the bonding condition, conductivity, and electron delocalization degree through the synergistic effect of heteroatoms, from the introduction of N, P, B, and halogen,[9−12] etc. into this sp−sp^2 rich-carbon framework.

More importantly, in 2012, researchers found that metal elements could effectively modulate the electrical properties of GDY, which included the redistribution of electron orbitals and the efficient electron transfer between metal and GDY caused by a strong coupling effect.[2,13−15] Beyond that, density functional theory (DFT) calculations also prove that the structure of −C≡C−metal−C≡C− can significantly improve GDY electronic properties,[16−18] which jointly show that the metallization engineering is an effective strategy for further enhancing the catalytic performance.[19−22] Meantime, the GDY with naturally distributed cavity structures and rich carbon atoms displays a high affinity with metal atoms.[23−25] Therefore, metalated-GDY has drawn increasing interest. However, the research on the efficient synthesis of metalated GDY is still in its infancy. At present, the introduction of metal atoms is mainly completed by inserting the external metal species into the defects and vacancies of GDY.[26−28] Metalated-GDY, for instance, has been obtained by surface polymerization under ultrahigh vacuum conditions, on a single crystal metal surface.[29−31] These methods have strict requirements for reaction conditions and are difficult to be applied in practical application. In addition, the alkynophilicity of silver has been reported.[32] This alkynophilicity is caused by Ag d^{10} electronic configuration and is beneficial for the reaction between silver and carbon−carbon bonds in alkynes.[32] Based on these, we attempt to introduce silver atoms into GDY through a simple wet chemical method.

Herein, a silver coordinated GDY (Ag-GDY) with excellent photoelectric characteristics and visible light absorption up to ca. 518 nm, corresponding to an optical bandgap of 2.61 eV, was synthesized through a simple wet-chemistry method. The excellent response to visible light and good conductivity of 2.6

Received: February 3, 2023
Accepted: April 19, 2023
Published: April 29, 2023

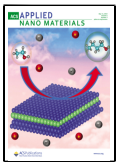

https://doi.org/10.1021/acsanm.3c00514
ACS Appl. Nano Mater. 2023, 6, 7395−7403

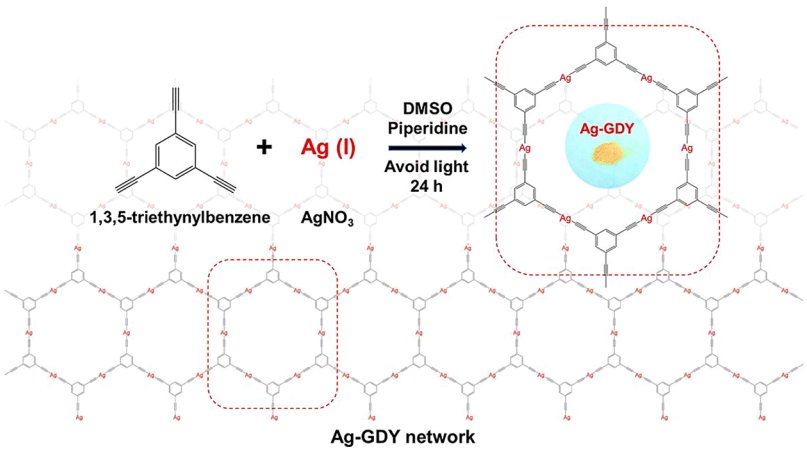

Figure 1. Chemical structures of the ligands and Ag-GDY.

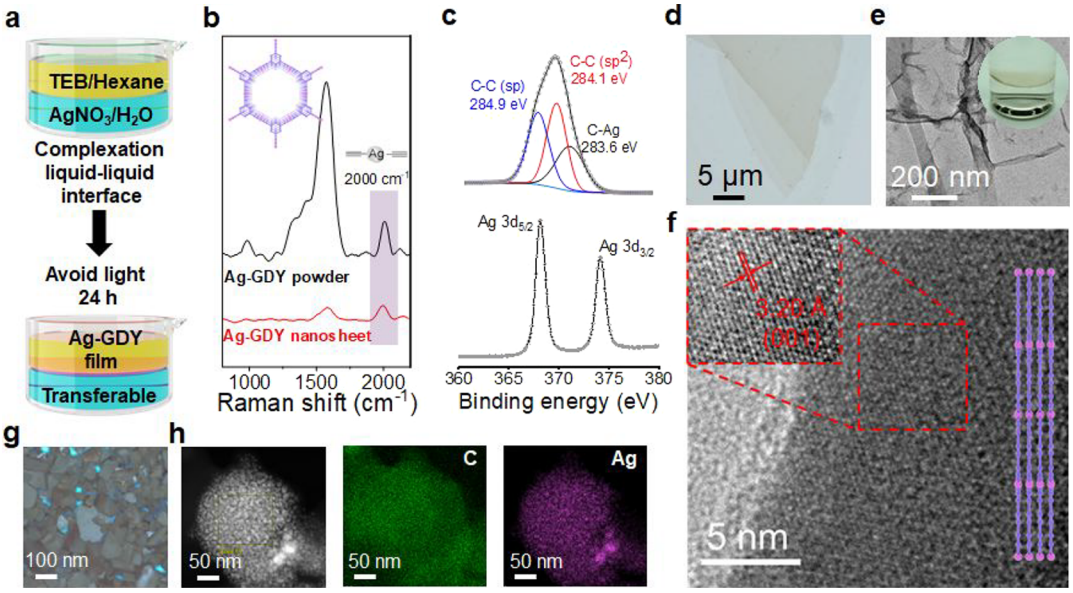

Figure 2. The synthesis, structure, and morphology of Ag-GDY. (a) Schematic diagram of the Ag-GDY film preparation. (b) Raman spectra of Ag-GDY. (c) High-resolution C 1s (top) and Ag 3d (bottom) core level spectra of Ag-GDY. (d) Optical photo of Ag-GDY film. (e) TEM image of Ag-GDY film on a Si wafer and photograph of Ag-GDY film at an interface (inside). (f) HRTEM image of Ag-GDY. (g) Optical photo of Ag-GDY powder. (h) SEM image of Ag-GDY powder and element mapping of Ag-GDY powder for C and Ag on Si wafer.

$\times 10^{-4}$ S cm^{-1} motivated the investigation of this material for photocatalysis. Ag-GDY showed outstanding photocatalytic performance degrading the organic antibiotic tetracycline and a dye. A low dose of Ag-GDY at 0.5 g L^{-1} resulted in 78% of tetracycline at 5×10^{-5} M in 1 h. Moreover, Ag-GDY retained its original structure after five replicate experiments demonstrating this material's great economic benefits and application prospects.

2. EXPERIMENTAL SECTION

2.1. Synthesis of Ag-GDY Powder and Film. An amount of 30 mg of 1,3,5-tri(phenylethynyl)benzene (TEB) was dissolved in 20 mL of DMSO. Then, 15 μL of piperidine was added as the alkali. Let the solution stand in the dark for 1 h. Subsequently, 17 mg of $AgNO_3$ was added, and the off-white floccule appeared. The reaction mixture was stirred for 24 h. The yellow precipitate was washed several times using acetone after drying for subsequent tests.

A 1,3,5-triethynylbenzene hexane solution (1 mM) and a silver nitrate aqueous solution (1 mM) were layered, and the reaction system was kept undisturbed and light-proof for 24 h. After the reaction, it can be seen that the light-yellow film is suspended in the middle of the interface. Then, the film was transferred onto a Si wafer through the Langmuir–Schäfer method. The film was washed several times using acetone after drying for subsequent tests.

2.2. PEC Measurements. The PEC performance of Ag-GDY-based photocathodes was tested using a three-electrode setup containing a working electrode (Ag-GDY on ITO glass), a counter electrode (Pt tablet), and a reference electrode (Ag/AgCl). The irradiation source was a 300 W Xe lamp coupled with an optical filter (λ > 420 nm). All the PEC measurements were performed on an electrochemical workstation (CHI 660 E, Chenhua Shanghai). 0.5 M Na_2SO_4 was used as an electrolyte. The EIS spectra were recorded by applying an A.C. The impedance pattern in the frequency ranges from 100 K to 0.01 Hz at a DC bias of −0.6 V vs Ag/AgCl. The current density was calculated using an exposed surface area of 1.0 cm^2 of photoelectrode:

$$J\ (\text{photocurrent density}) = J\ (\text{measured photocurrent})/S\ (\text{exposed surface area})$$

The Mott–Schottky plots were recorded by applying an impedance-potential pattern in the frequency of 500, 1000, and

https://doi.org/10.1021/acsanm.3c00514
ACS Appl. Nano Mater. 2023, 6, 7395−7403

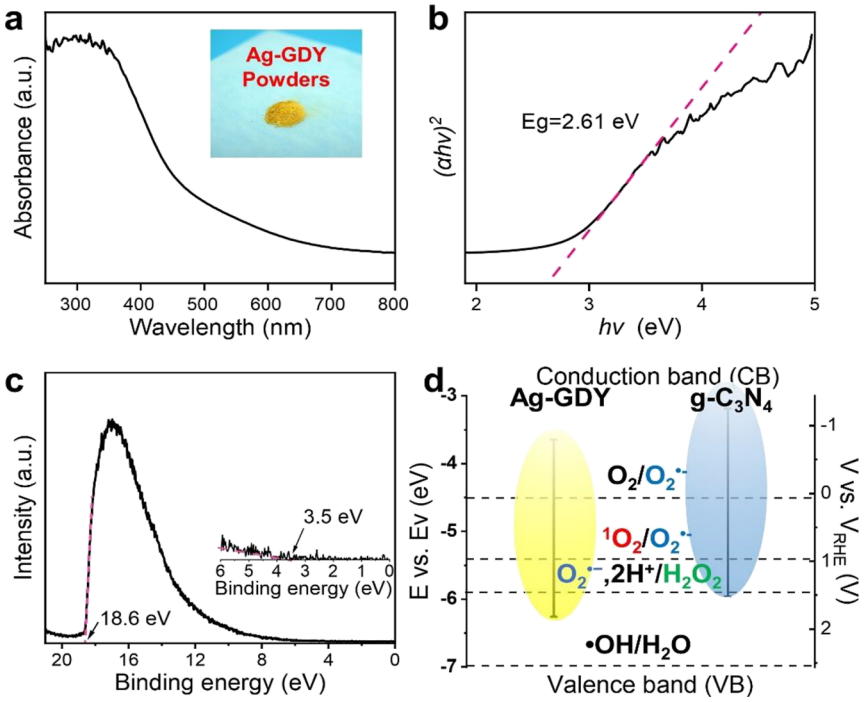

Figure 3. Optical absorption spectrum and energy band structure. (a) UV−vis absorption spectrum of Ag-GDY. (b) Tauc plot shows the Ag-GDY bandgap: E_g = 2.61 eV. (c) UPS spectrum. The width of UPS can be determined according to the intersection of left and right tangents and baseline. (d) Comparison diagram of the energy band structure of Ag-GDY and g-C_3N_4.

1500 Hz, respectively. The applied potential vs Ag/AgCl is converted to RHE potential using the following equation:

$$E_{RHE} = 0.05916\ pH + E_{Ag/AgCl}{}^{0}\ (E_{Ag/AgCl}{}^{0} = 0.199\ V) + E_{Ag/AgCl}$$

2.3. Photocatalytic Degradations of Tetracycline (TC) and Rhodamine B (RhB). The photocatalytic degradations of RhB and TC: 10 mg of Ag-GDY was suspended in 20 mL of RhB DI aqueous solution (5.0×10^{-5} M) and TC DI aqueous solution (5.0×10^{-5} M), respectively. The light source was a 300 W Xe lamp (CEL-HXF300-T3) equipped with a cutoff filter of 420 nm < λ < 800 nm, and the reaction was carried out at 20 °C. Before irradiation, the suspension was stirred in the dark for 1 h to reach adsorption−desorption equilibrium. At certain time intervals (RhB: 10 min, TC: 10 min), 2 mL of solution was sampled. The photocatalyst was separated by centrifugation, and then the absorbance of the supernatant was recorded on a UV-1800 spectrophotometer. The absorbance was recorded at 554 nm for RhB and at 358 nm for TC. Cycling experiments were also carried out in the same manner.

3. RESULTS AND DISCUSSION

3.1. Synthesis and Characterization of Ag-GDY Powder and Film. The ligand of 1,3,5-triethynylbenzene was used to synthesize Ag-GDY (Figure 1) through a base-catalyzed dehydrohalogenation reaction. The dimethyl sulfoxide solution contained $AgNO_3$, piperidine, and 1,3,5-triethynylbenzene reacted at room temperature (Figure S1).[33] Besides, the Ag-GDY film was synthesized by liquid/liquid interfacial polymerization (Figure 2a).[33] The obtained film could be easily transferred to any substrate. The Raman spectrum of the resulting material showed neither the characteristic peak of the terminal alkyne group (2212 cm^{-1}) nor the characteristic peak of the diyne bond (2106 cm^{-1}),[34] but a new peak (2006 cm^{-1}) (Figure 2b) appeared, which can be attributed to C≡C stretching caused by C−Ag[35]. X-ray photoelectron spectroscopy (XPS) results confirm that Ag was successfully introduced into GDY (Figure S2). The high-resolution C 1s XPS spectra of Ag-GDY (Figure 2c) were deconvoluted into C−C (sp, 284.9 eV), C−C (sp^2, 284.1 eV), and C−Ag (sp, 283.6 eV),[33,35] which is consistent with the Raman spectroscopy results evidencing successful construction of the Ag-coordinated sp−sp^2 hybridized carbon network. Two peaks at 368.2 and 374.1 eV (Figure 2c) in the high-resolution Ag 3d XPS spectra could be assigned to the uniform bonding of Ag(I) with the carbon-rich framework.[36] In addition, FTIR spectra of Ag-GDY (Figure S3) also proved the introduction of Ag. The sharp peak at about 3280 cm^{-1} for the ≡C−H stretching vibrations disappeared, and the shifting of the peak at about 2110 cm^{-1} for C≡C indicated that the metal alkynylation reaction occurred.[37]

The following considerations may explain the reaction pathway: (i) the piperidine and triethylamine as alkali-agents promote the dehydrogenation of terminal alkynes; (ii) the dehydrogenated terminal alkynes bond with Ag(I) to form a metal−organic complex compound; and (iii) the metal−organic complex compound further reacts with the dissociative terminal alkynes to create the grapdiyne-like framework.[35]

Optical microscopy (Figures 2d and S4), scanning probe microscopy (SPM), scanning electron microscopy (SEM) (Figure S5), and transmission electron microscopy (TEM) (Figures 2c and S6) were used to characterize the Ag-GDY samples' microstructure. The optical and SPM images (Figures 2d and S7) showed the successful transfer of Ag-GDY with a 2D nanostructure, from about 5 to 15 nm. SEM (Figure 2d) and TEM imaging (Figure 2e) results showed the few-layered structure of Ag-GDY with folds and curls. Furthermore, the Ag-GDY film crystallinity was studied through high-resolution TEM (HRTEM) (Figure 2f), showing an interlayer spacing of about 3.20 Å. The mentioned results are very close to that of graphene (3.35 Å) and GDY (3.65 Å).[38] The crystal structure

https://doi.org/10.1021/acsanm.3c00514
ACS Appl. Nano Mater. 2023, 6, 7395−7403

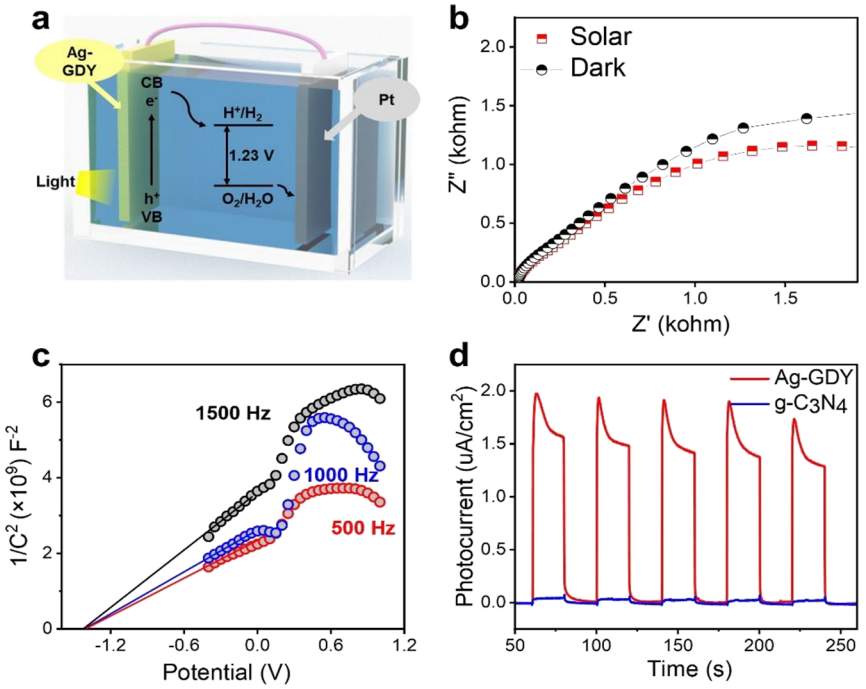

Figure 4. PEC characterization. (a) PEC cell with an Ag-GDY photocathode under visible light irradiation. (b) EIS Nyquist plots of Ag-GDY at a voltage of −0.6 V vs Ag/AgCl under dark (black point) and light (red point), respectively. (c) Mott−Schottky plots of Ag-GDY at a voltage of −0.4 V vs Ag/AgCl with a frequency of 500 Hz (red curve), 1000 Hz (blue curve), and 1500 Hz (black curve). (d) Transient current density vs time at 0 V vs Ag/AgCl for Ag-GDY and g-C_3N_4.

of Ag-GDY powder was revealed by powder X-ray diffraction (XRD). The XRD result (Figure S8) showed diffraction peaks at 2θ angles of 9.0, 23.5, and 27.7°, which were assigned to (100), (200), and (001) planes, respectively.[33] (100) and (200) reflection planes revealed a long-range order within the ab plane, and (001) reflections revealed the existence of $\pi-\pi$ stacking between the individual layer. The wider peak at 27.7° indicates that the layer distance between two individual metalized frameworks is 3.23 Å, in close agreement with HRTEM results. The morphology of yellow Ag-GDY powder observed by SEM (Figure 2g) indicated that the Ag-GDY powder is characterized by a porous and loose microstructure, which is excellent for enhancing contact with pollutants. The elemental mapping distribution in Figure 2h shows that C and Ag are well-dispersed throughout the Ag-GDY sample, which is also consistent with XPS analysis.

Thermogravimetric analysis (TG) (Figure S9) showed that the Ag-GDY powder decomposition temperature is about 180 °C, indicating its good thermal stability. The Ag-GDY powder porosity was evaluated from Argon adsorption−desorption isotherms (Figure S10), showing a surface area of 102.9 $m^2\ g^{-1}$ with most pore sizes at 1.71 nm. These results are consistent with SEM images of Ag-GDY powder.

3.2. Optical and Electronic Structure Characterization. To evaluate the absorption edge and band gap of Ag-GDY, the ultraviolet−visible (UV−vis) absorption spectrum (Figure 3a) was recorded. The Ag-GDY showed an absorption edge of about 518 nm with a narrow band gap of 2.61 eV deduced from the Tauc plot in Figure 3b. This result is significant since it shows that Ag-GDY could absorb visible light and thus be excited by it. The broad absorption edge and narrow band gap were due to metal polarization that reduced the electron density.[35] In addition, ultraviolet photoelectron spectroscopy (UPS) (Figure 3c) was carried out to jointly evaluate the energy level of the valence band (E_{vb}) of Ag-GDY. The E_{vb} 6.26 eV was calculated by the following formula: $E_{vb} = h\nu$ (HeI, 21.21 eV) − W (width of UPS).[34,35] The energy level of the conduction band (E_{cb}) 3.65 eV was obtained from the band gap width and E_{vb}. As shown in Figure 3d, these values (with respect to the vacuum level) could be converted into electrochemical potentials such that E_{vb} and E_{cb} are 1.82 V vs RHE and −0.79 V vs RHE, respectively.[39] In addition, Ag-GDY exhibits a bandgap close to GDY (Figure S11) and a narrower band gap than commonly used organic photocatalysts g-C_3N_4.[35] All these results demonstrate that the suitable energy band structure of Ag-GDY is conducive to electron and hole separation, promoting photocatalytic performance.

3.3. Photoelectrochemistry Characterization. It was well known that the separation efficiency of electrons and holes was directly linked with photocatalytic efficiency. Based on this, we carried out a series of photoelectrochemistry (PEC) tests. The PEC tests were performed with Ag-GDY coated on indium tin oxide (ITO) glass as the photocathode in 0.5 M Na_2SO_4 electrolyte. The three-electrode system was completed with Ag/AgCl as the reference electrode and glassy carbon and platinum foil as counter electrodes (Figure 4a). Electrochemical impedance spectroscopy (EIS) was carried out to explore interfacial charge transfer. EIS curves (Figure 4b) revealed a reduced charge-transport resistance of Ag-GDY under light irradiation, which means that light improves Ag-GDY conductivity. The Mott−Schottky plots (Figure 4c) of Ag-GDY helped us understand the band structure of Ag-GDY, which showed an intercept at −1.4 V vs Ag/AgCl. By matrixing, the conduction band of Ag-GDY was evaluated at −0.79 V vs RHE.[39,40] By taking the band gap into account, the valence band is 1.82 V vs RHE. These values approximate the UPS results. The current−time curve (Figure 4d) showed a

https://doi.org/10.1021/acsanm.3c00514
ACS Appl. Nano Mater. 2023, 6, 7395−7403

remarkable change when the light source was switched on and off, which proved that the Ag-GDY had a rapid response to light. It was apparent that the photocurrent intensity of Ag-GDY far exceeded g-C_3N_4, which indicates an outstanding light absorption ability and a superior e^-/h^+ separation efficiency for Ag-GDY. The photocurrent decreased gradually after reaching the maximum value, which might be caused by the gradual reduction of the separation efficiency of photogenerated electrons and holes.

3.4. Conductivity Measurement. To quantify the electrical conductivity and light response of Ag-GDY film, we used the well-known van der Pauw method to measure the dark film conductivity and the conductivity change under different light excitation wavelengths. The sample was first grown in a liquid/liquid interface and fished out of the solution using a plasma-activated silicon wafer plated with gold contacts (Figure 5a).

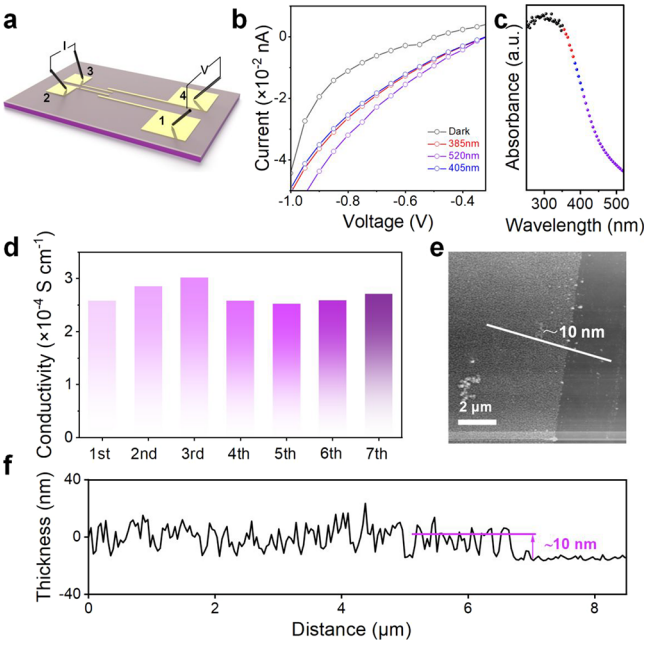

Figure 5. Conductivity tests of Ag-GDY film. (a) Schematic of four-probe system devices for conductivity measurement. (b) Change of conductivity under light irradiation with different wavelengths. (c) UV−vis adsorption spectrum of Ag-GDY. (d) SPM image of film loaded on devices. (e) Thickness of Ag-GDY film loaded on a device. (f) Conductivity and repetitive stability measured by the four-probe system.

To test the effect of light on conductivity, two probes were connected to the smaller electrodes. One probe was biased, and the other was voltage-measured. The test results showed that the introduction of light was conducive to increasing the conductivity of Ag-GDY film (Figure 5b). Compared with the conductivity in the dark state, the conductivity is improved significantly under the light irradiation of 385, 405, and 520 nm wavelengths (Figure 5b,c). The following reasons could explain this phenomenon: Ag-GDY film absorbed more protons in the ultraviolet and the near-ultraviolet band, which caused more electrons to be excited and separated from holes, leading to a more pronounced conductivity increase.[41] For the electrical characterization, two probes connected to the larger electrodes were assigned for the current bias (terminals 1 and 4). The other two probes at the opposite larger electrode measured the voltage (terminals 2 and 3). The conductivity (σ) is calculated by the following formula:

$$\sigma = \frac{(I \times L)}{W \times D \times (V_2 - V_3)}$$

Where L is the distance between the two larger electrodes, W is the length of the larger electrodes, and D is the film thickness (Figure S12). The average Ag-GD film conductivity was about 2.6×10^{-4} S cm^{-1}. The conductivity did not change significantly after seven repeated tests, indicating excellent film stability (Figure 5d). The film thickness was controlled at about 10 nm to eliminate the thickness effects on conductivity (Figure 5e,f).

3.5. Photocatalytic Activity of Ag-GDY. Industrial wastewater discharge, such as dyes into the water, endanger aquatic organisms' survival and cause environmental pollution. Antibiotic residues also have biological toxicity, which causes harm to aquatic organisms, also harming humans through the food chain.[42,43] Therefore, removing dyes and antibiotics is crucial for environmental protection. To show the impact of our material on ecological remediation, the degradation of rhodamine B (RhB) and tetracycline (TC) was explored in water under visible light by using Ag-GDY as a photocatalyst.

The photocatalytic activity of Ag-GDY was evaluated from the degradation of dyes and antibiotics under visible light (λ > 420 nm). The photocatalytic performance of Ag-GDY was compared with two common commercial photocatalytic materials, P25, g-C_3N_4 and pristine GDY. Ag-GDY displayed the best activity for the degradation of RhB with complete degradation after 30 min. In contrast, the degradation efficiency of P25 and g-C_3N_4 reached only 34% for the same period, and GDY exhibits a slightly lower photocatalytic efficiency than Ag-GDY by about 10% (Figure 6a). The P25-induced degradation of RhB under visible light is attributed to dye-sensitization.[39] For the degradation of tetracycline, Ag-GDY also showed excellent photocatalytic ability. After 30 min, Ag-GDY degraded 78% of tetracycline, which is superior to other photocatalysts that reached only 37, 11, and 9% with P25, g-C_3N_4, and pristine GDY, respectively (Figure 6b). It is worth noting that tetracycline could also sensitize P25 and display photocatalytic activity under visible light.[43,44] We compared the degradation ability of Ag-GDY with different silver ratios for tetracycline and found that their changes were not significant, which also proves that the silver element enters the graphdiyne frameworks in the form of bonding rather than doping (Figure S14). In addition, compared with other reported 2D materials, Ag-GDY also exhibits the best photocatalytic performance (Table S1). Among them, Ag-GDY exhibits excellent photocatalytic performance for both RhB and TC, which is attributed to its better light absorption ability, carrier conductivity, and carrier separation efficiency.

Additional tests were carried out to study the recyclability of Ag-GDY. The cycle stability test (Figure S12) indicated that Ag-GDY maintained excellent photocatalytic activity after five reuse cycles, proving that Ag-GDY had excellent cycling stability, and reusability. This characteristic is essential for practical applications and economic benefits. The superb stability was also confirmed by post-reaction Raman spectra (Figure S15) and the XRD patterns (Figure S16), which prove that the Ag-GDY structure remained unchanged. All these results indicate that Ag-GDY is an efficient and stable

https://doi.org/10.1021/acsanm.3c00514
ACS Appl. Nano Mater. 2023, 6, 7395−7403

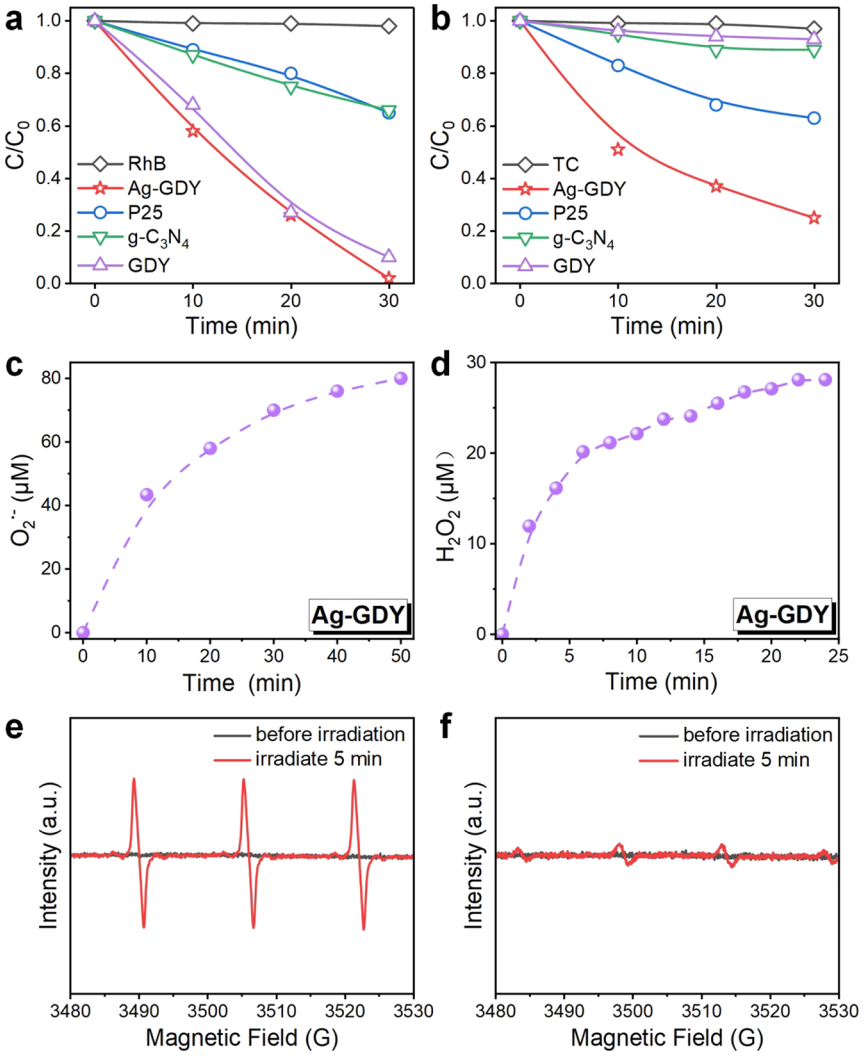

Figure 6. Photocatalytic degradation diagram and free radical characterization. (a) Photocatalytic degradation of RhB (C_{RhB} = 5.0 × 10^{-5} M, $C_{Ag\text{-}GDY}$ = 0.5 g L^{-1}). (b) Photocatalytic degradation of TC (C_{TC} = 5.0 × 10^{-5} M, $C_{Ag\text{-}GDY}$ = 0.5 g L^{-1}). (c) Photocatalytic production of $O_2^{\cdot-}$ by Ag-GDY. (d) Photocatalytic production of H_2O_2 by Ag-GDY. (e) EPR diagram of $^1O_2$ before and after illumination. (f) EPR diagram of $^{\cdot}OH$ before and after illumination.

photocatalyst for eliminating dyes and antibiotics from water. However, the post-reaction SEM analysis (Figure S17) of Ag-GDY showed that the powder tended to change from loose to tight, which might affect the molecular adsorption of Ag-GDY rather than its photocatalytic performance.

3.6. Photocatalytic Mechanism of Ag-GDY. The photocatalytic pathway is based on the photogeneration of charge carriers and their separation into electrons (e^-) and holes (h^+) to drive chemical reactions. When a semiconductor is illuminated by light with energy higher than its band gap, electrons in the valence band are excited to the conduction band, leaving holes behind in the valence band. These carriers then migrate to the semiconductor surface.[44] If the semiconductor were in an environment containing oxygen and water, the electrons migrating to the surface of the semiconductor would react with water and oxygen to form highly oxidizing free radicals, which could degrade pollutants, such as dye and antibiotics.[45] A series of control experiments were carried out to identify the free radicals produced in the photocatalysis process. Oxygen molecules were activated into $O_2^{\cdot-}$, accepting electrons from the conduction band. According to the characteristic reaction of nitrotetrazolium blue chloride (NBT),[46−48] we could quantitatively analyze the generation of $O_2^{\cdot-}$ under light irradiation. The results show that after 50 min, about 8.0 μM of $O_2^{\cdot-}$ was produced in the aqueous suspension (Figure 6c). About 4.6 μM of H_2O_2 was produced by protonation of $O_2^{\cdot-}$, which was also detected by N,N-diethyl-*p*-phenylenediamine (DPD)−horseradish peroxidase (POD) method (Figure 6d).[48,49] Generation of $^1O_2$ was detected by electron paramagnetic resonance (EPR) spectrum in the aqueous suspension (Figure 6e), with 2,2,6,6-tetramethyl-4-piperidone (TEMP) as the spin-trapping agent. In addition, photogenerated electrons and a small amount of $^{\cdot}OH$ were detected by EPR, with 2,2,6,6-Tetramethylpiperidinooxy (TEMPO) and 5,5-dimethyl-1-pyrroline-N-oxide (DMPO) as spin-trapping agents, respectively (Figures 6f and S16).[48] The formation process of these radicals could be explained by the following reactions eqs 1−6:

$$O_2 + e^- \rightarrow O_2^{\cdot-} \quad (1)$$

$$O_2^{\cdot-} + H^+ \rightarrow HO_2\cdot \quad (2)$$

$$2HO_2\cdot \rightarrow H_2O_2 + O_2 \quad (3)$$

https://doi.org/10.1021/acsanm.3c00514
ACS Appl. Nano Mater. 2023, 6, 7395−7403

$$H_2O_2 + O_2^{\cdot-} \rightarrow {}^{\cdot}OH + O_2 + HO^- \quad (4)$$

$$H_2O_2 + h\nu \rightarrow 2\,{}^{\cdot}OH \quad (5)$$

$$O_2^{\cdot-} + h^+ \rightarrow {}^1O_2 \quad (6)$$

According to the valence band energy level, ·OH should not have been produced in theory, but a small amount of ·OH was still detected by EPR, which was produced according to eqs 4 and 5.[48] All of these results show that the reactive oxygen species (ROS) production was induced by photogenerated electrons and photogenerated holes generated from Ag-GDY.

To clarify the contribution of ROS to the photodegradation under visible light irradiation, three scavengers (BQ, t-BuOH, and MeOH) were used to quench $O_2^{\cdot-}$, ·OH, and h^+, respectively[50,51] As shown in Figure S18, the addition of tert-butanol (t-BuOH) did not change the degradation efficiency of RhB, which was consistent with the EPR results, indicating that ·OH was not the main active species. With the introduction of 1,4-benzoquinone (BQ), the degradation efficiency of RhB decreased significantly from 99.9 to 54.5%, illustrating that $O_2^{\cdot-}$ made a major contribution to photocatalysis. When methanol (MeOH) was added, the degradation efficiency of RhB decreased dramatically to 46.6%, demonstrating that h^+ also played an important role. Considering that $^1O_2$ may come from the oxidation of holes, we deemed that $^1O_2$ also has a good degradation effect on pollutants.

We propose a pollutant degradation mechanism based on the energy band structure of Ag-GDY, EPR spectra, and scavenger experimental results. As shown in Figure 7, visible

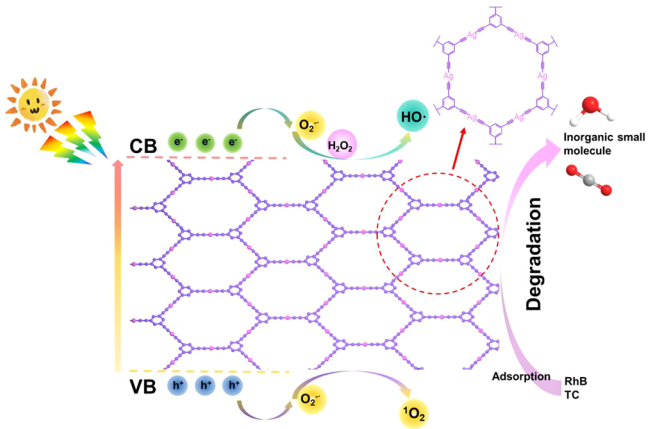

Figure 7. Mechanism diagram of visible light photocatalytic degradation of pollutants.

light could excite the electrons from the valence band to the conduction band with holes generated in the valence band. The electrons further transfer to the Ag-GDY surface and then react with O_2 to form $O_2^{\cdot-}$, which degrades the pollutant adsorbed on Ag-GDY to inorganic small molecules. In aqueous conditions, $O_2^{\cdot-}$ could further react with H^+ to produce H_2O_2, which could be oxidized by $O_2^{\cdot-}$ to ·OH, but as we already showed, ·OH was not the main active species in the photocatalytic reaction. The h^+ could directly oxidize the adsorbed pollutants or oxidized $O_2^{\cdot-}$ to form more active $^1O_2$. The calculated energy band structure also confirmed the theoretical feasibility of this degradation pathway.

4. CONCLUSIONS

In this study, we reported robust and fast methodologies for synthesizing Ag-GDY. The as-prepared Ag-GDY had an appropriate bandgap at 2.61 V and a broad optical absorption edge reaching 518 nm. PEC and film conductivity tests showed that Ag-GDY has good light response characteristics and charge transfer ability. Furthermore, the Ag-GDY displayed excellent photocatalytic performance for degrading dyes and antibiotics and illustrated good cycle stability. Through the characteristic reaction and quencher control experiments, we identified and quantified the free radicals that make major contributions to the photocatalytic process. We elucidated a possible photocatalytic reaction pathway based on the deduced band structure of the material and control experiments. These results showed that Ag-GDY opens a broad development prospect for metallized conjugated carbon materials in photocatalysis with an emphasis on ecological remediation.

■ ASSOCIATED CONTENT

Supporting Information

The Supporting Information is available free of charge at https://pubs.acs.org/doi/10.1021/acsanm.3c00514.

Schematic diagram, XPS, FTIR, optical microscope images, SEM, TEM, AFM, XRD, TG, and nitrogen adsorption/desorption isotherms (PDF)

■ AUTHOR INFORMATION

Corresponding Authors

Tao Wang − *School of Materials Science and Engineering, Zhejiang Sci-Tech University, Hangzhou 310018, China*; Email: taotao571@hotmail.com

Tao Zhang − *Key Laboratory of Marine Materials and Related Technologies, Ningbo Institute of Materials Technology and Engineering, Chinese Academy of Sciences, Ningbo 315201, China*; orcid.org/0000-0003-3218-0571; Email: tzhang@nimte.ac.cn

Authors

Runhao Huang − *School of Materials Science and Engineering, Zhejiang Sci-Tech University, Hangzhou 310018, China; Key Laboratory of Marine Materials and Related Technologies, Ningbo Institute of Materials Technology and Engineering, Chinese Academy of Sciences, Ningbo 315201, China*; orcid.org/0000-0002-5157-6304

Zhenhui Kou − *Key Laboratory of Marine Materials and Related Technologies, Ningbo Institute of Materials Technology and Engineering, Chinese Academy of Sciences, Ningbo 315201, China*

Raul D. Rodriguez − *Tomsk Polytechnic University, Tomsk 634050, Russia*

Xusheng Wang − *Institute of Functional Porous Materials, School of Materials Science and Engineering, Zhejiang Sci-Tech University, Hangzhou 310018, China*

Yang Hou − *College of Chemical and Biological Engineering, Zhejiang University, Hangzhou, Zhejiang 310027, China*; orcid.org/0000-0001-9795-8503

Complete contact information is available at: https://pubs.acs.org/10.1021/acsanm.3c00514

Author Contributions

#R.H. and Z.K. contributed equally to this work.

https://doi.org/10.1021/acsanm.3c00514
ACS Appl. Nano Mater. 2023, 6, 7395−7403

Notes

The authors declare no competing financial interest.

■ ACKNOWLEDGMENTS

T. Z. acknowledges the Excellent Youth Foundation of Zhejiang Province of China (Grant No. LR21E030001), the Leading Innovative and Entrepreneur Team Introduction Program of Zhejiang (2021R01005), and the National Natural Science Foundation of China (Grant Nos. 52003279). R.D.R. acknowledges the RFBR project number 21-53-12045.

■ REFERENCES

(1) Li, Y. J.; Xu, L.; Liu, H. B.; Li, Y. L. Graphdiyne and graphyne: from theoretical predictions to practical construction. *Chem. Soc. Rev.* **2014**, *43*, 2572−2586.
(2) Gao, X.; Liu, H. B.; Wang, D.; Zhang, J. Graphdiyne: synthesis, properties, and applications. *Chem. Soc. Rev.* **2019**, *48*, 908−936.
(3) Sun, H. J.; Oner, I. H.; Wang, T.; Zhang, T.; Selyshchev, O.; Neumann, C.; Fu, Y. B.; Liao, Z. Q.; Xu, S. Q.; Hou, Y.; Turchanin, A.; Zahn, D. R. T.; Zschech, E.; Weidinger, I. M.; Zhang, J.; Feng, X. L. Molecular Engineering of Conjugated Acetylenic Polymers for Efficient Cocatalyst-free Photoelectrochemical Water Reduction. *Angew. Chem., Int. Ed.* **2019**, *58*, 10368−10374.
(4) Li, S. X.; Ma, R.; Xu, S. Q.; Zheng, T. Y.; Fu, G. E.; Wu, Y. L.; Liao, Z. Q.; Kuang, Y. B.; Hou, Y.; Wang, D. S.; Petkov, P. S.; Simeonova, K.; Feng, X. L.; Wu, L. Z.; Li, X. B.; Zhang, T. Direct Construction of Isomeric Benzobisoxazole-Vinylene-Linked Covalent Organic Frameworks with Distinct Photocatalytic Properties. *J. Am. Chem. Soc.* **2022**, *144*, 13953−13960.
(5) Xing, C. Y.; Xue, Y. R.; Huang, B. L.; Yu, H. D.; Hui, L.; Fang, Y.; Liu, Y. X.; Zhao, Y. J.; Li, Z. B.; Li, Y. L. Fluorographdiyne: A Metal-Free Catalyst for Applications in Water Reduction and Oxidation. *Angew. Chem., Int. Ed.* **2019**, *58*, 13897−13903.
(6) Chae, H. K.; Siberio-Perez, D. Y.; Kim, J.; Go, Y.; Eddaoudi, M.; Matzger, A. J.; O'Keeffe, M.; Yaghi, O. M. A route to high surface area, porosity and inclusion of large molecules in crystals. *Nature* **2004**, *427*, 523−527.
(7) Long, M. Q.; Tang, L.; Wang, D.; Li, Y. L.; Shuai, Z. G. Electronic Structure and Carrier Mobility in Graphdiyne Sheet and Nanoribbons: Theoretical Predictions. *ACS Nano* **2011**, *5*, 2593−2600.
(8) Wang, N.; He, J. J.; Wang, K.; Zhao, Y. J.; Jiu, T. G.; Huang, C. S.; Li, Y. L. Graphdiyne-Based Materials: Preparation and Application for Electrochemical Energy Storage. *Adv. Mater.* **2019**, *31*, No. 1803202.
(9) Shen, X. Y.; Li, X. D.; Zhao, F. H.; Wang, N.; Xie, C. P.; He, J. J.; Si, W. Y.; Yi, Y. P.; Yang, Z.; Li, X. F.; Lu, F. S.; Huang, C. S. Preparation and structure study of phosphorus-doped porous graphdiyne and its efficient lithium storage application. *2D Materials* **2019**, *6*, No. 035020.
(10) Zhao, Y. S.; Yang, N. L.; Yao, H. Y.; Liu, D. B.; Song, L.; Zhu, J.; Li, S. Z.; Gu, L.; Lin, K. F.; Wang, D. Stereodefined Codoping of sp-N and S Atoms in Few-Layer Graphdiyne for Oxygen Evolution Reaction. *J. Am. Chem. Soc.* **2019**, *141*, 7240−7244.
(11) Zhao, J.; Chen, Z.; Zhao, J. X. Metal-free graphdiyne doped with sp-hybridized boron and nitrogen atoms at acetylenic sites for high-efficiency electroreduction of CO_2 to CH_4 and C_2H_4. *J. Mater. Chem. A* **2019**, *7*, 4026−4035.
(12) Zou, H. Y.; Rong, W. F.; Long, B. H.; Ji, Y. F.; Duan, L. L. Corrosion-Induced Cl-Doped Ultrathin Graphdiyne toward Electrocatalytic Nitrogen Reduction at Ambient Conditions. *ACS Catal.* **2019**, *9*, 10649−10655.
(13) Wang, Z. Q.; Zheng, Z. Q.; Xue, Y. R.; He, F.; Li, Y. L. Acidic Water Oxidation on Quantum Dots of IrO_x/Graphdiyne. *Adv. Energy Mater.* **2021**, *11*, No. 2101138.
(14) Fang, M.; Xu, L.; Zhang, H.; Zhu, Y.; Wong, W.-Y. Metalloporphyrin-Linked Mercurated Graphynes for Ultrastable CO_2 Electroreduction to CO with Nearly 100% Selectivity at a Current Density of 1.2 A cm^{-2}. *J. Am. Chem. Soc.* **2022**, *144*, 15143−15154.
(15) He, J. J.; Ma, S. Y.; Zhou, P.; Zhang, C. X.; He, C. Y.; Sun, L. Z. Magnetic Properties of Single Transition-Metal Atom Absorbed Graphdiyne and Graphyne Sheet from DFT plus U Calculations. *J. Phys. Chem. C* **2012**, *116*, 26313−26321.
(16) Chen, X. L.; He, F.; Fang, W. N.; Shen, J. L.; Liu, X. G.; Xue, Y. R.; Liu, H. B.; Li, J.; Wang, L. H.; Li, Y. L.; Fan, C. H. DNA-Guided Room-Temperature Synthesis of Single-Crystalline Gold Nanostructures on Graphdiyne Substrates. *ACS Central Sci.* **2020**, *6*, 779−786.
(17) Tu, X. C.; Wang, H.; Shen, Z. Y.; Wang, Y. F.; Sanvito, S.; Hou, S. M. Cu-metalated carbyne acting as a promising molecular wire. *J. Chem. Phys.* **2016**, *145*, 244702.
(18) Hu, X. L.; Xiong, L. X.; Fang, W. H.; Su, N. Q. Computational Insight into Metallated Graphynes as Single Atom Electrocatalysts for Nitrogen Fixation. *ACS Appl. Mater. Interfaces* **2022**, *14*, 27861−27872.
(19) Li, T.; Jin, Z. L. Rationally engineered avtive sites for efficient and durable hydrogen production over γ-graphyne assembly $CuMoO_4$ S-scheme heterojunction. *J. Catal.* **2023**, *417*, 274−285.
(20) Jin, Z. L.; Li, X. H.; Li, T.; Li, Y. J. Graphdiyne (C_nH_{2n-2})-Based GDY/CuI/MIL-53(Al) S-Scheme Heterojunction for Efficient Hydrogen Evolution. *Langmuir* **2022**, *38*, 15632−15641.
(21) Wang, X. Y.; Jin, Z. L. A novel graphdiyne (C_nH_{2n-2}) preparation strategy: calcium carbide-derived graphdiyne film supported cobalt tetroxide nanoneedles for photocatalytic hydrogen production. *J. Mater. Chem. A* **2022**, *10*, 23134−23144.
(22) Jin, Z.; Wu, Y. Novel preparation strategy of graphdiyne (C_nH_{2n-2}): One-pot conjugation and S-Scheme heterojunctions formed with MoP characterized with in situ XPS for efficiently photocatalytic hydrogen evolution. *Appl. Catal. B.* **2023**, *327*, No. 122461.
(23) Cretu, O.; Krasheninnikov, A. V.; Rodriguez-Manzo, J. A.; Sun, L. T.; Nieminen, R. M.; Banhart, F. Migration and Localization of Metal Atoms on Strained Graphene. *Phys. Rev. Lett.* **2010**, *105*, No. 196102.
(24) Mengxue Yang, Y. L.; Jin, Z. In situ XPS proved graphdiyne (C_nH_{2n-2})-based CoFe LDH/CuI/GD double S-scheme heterojunction photocatalyst for hydrogen evolution. *Sep. Purif. Technol.* **2023**, *311*, No. 123229.
(25) Qi, S. Y.; Wang, J. R.; Song, X. H.; Fan, Y. C.; Li, W. F.; Du, A. J.; Zhao, M. W. Synergistic trifunctional electrocatalysis of pyridinic nitrogen and single transition-metal atoms anchored on pyrazine-modified graphdiyne. *Sci. Bull.* **2020**, *65*, 995−1002.
(26) Zhao, J.; Deng, Q. M.; Bachmatiuk, A.; Sandeep, G.; Popov, A.; Eckert, J.; Rummeli, M. H. Free-Standing Single-Atom-Thick Iron Membranes Suspended in Graphene Pores. *Science* **2014**, *343*, 1228−1232.
(27) Wang, H. T.; Wang, Q. X.; Cheng, Y. C.; Li, K.; Yao, Y. B.; Zhang, Q.; Dong, C. Z.; Wang, P.; Schwingenschlogl, U.; Yang, W.; Zhang, X. X. Doping Monolayer Graphene with Single Atom Substitutions. *Nano Lett.* **2012**, *12*, 141−144.
(28) Fan, Y. C.; Yu, J. P.; Song, X. H.; Liu, Y.; Qi, S. Y.; Li, W. F.; Zhao, M. W. The role of sp-hybridized boron atoms in the highly efficient photocatalytic N_2 reduction activity of boron-doped triphenylene-graphdiyne. *J. Mater. Chem. A* **2021**, *9*, 26077−26085.
(29) Yang, Z. C.; Gebhardt, J.; Schaub, T. A.; Sander, T.; Schonamsgruber, J.; Soni, H.; Gorling, A.; Kivala, M.; Maier, S. Two-dimensional delocalized states in organometallic bis-acetylide networks on Ag(111). *Nanoscale* **2018**, *10*, 3769−3776.
(30) Sun, Q.; Cai, L. L.; Ma, H. H.; Yuan, C. X.; Xu, W. Dehalogenative Homocoupling of Terminal Alkynyl Bromides on Au(111): Incorporation of Acetylenic Scaffolding into Surface Nanostructures. *ACS Nano* **2016**, *10*, 7023−7030.
(31) Liu, P. X.; Qin, R. X.; Fu, G.; Zheng, N. F. Surface Coordination Chemistry of Metal Nanomaterials. *J. Am. Chem. Soc.* **2017**, *139*, 2122−2131.
(32) Fang, G. C.; Bi, X. H. Silver-catalysed reactions of alkynes: recent advances. *Chem. Soc. Rev.* **2015**, *44*, 8124−8173.

https://doi.org/10.1021/acsanm.3c00514
ACS Appl. Nano Mater. 2023, 6, 7395−7403

(33) Xu, L. L.; Sun, J. B.; Tang, T. H.; Zhang, H. Y.; Sun, M. Z.; Zhang, J. Q.; Li, J. H.; Huang, B. L.; Wang, Z. P.; Xie, Z.; Wong, W. Y. Metallated Graphynes as a New Class of Photofunctional 2D Organometallic Nanosheets. *Angew. Chem., Int. Ed.* **2021**, *60*, 11326−11334.
(34) Zhang, T.; Hou, Y.; Dzhagan, V.; Liao, Z. Q.; Chai, G. L.; Loffler, M.; Olianas, D.; Milani, A.; Xu, S. Q.; Tommasini, M.; Zahn, D. R. T.; Zheng, Z. K.; Zschech, E.; Jordan, R.; Feng, X. L. Copper-surface-mediated synthesis of acetylenic carbon-rich nanofibers for active metal-free photocathodes. *Nat. Commun.* **2018**, *9*, 1140.
(35) Zhang, T.; Xu, S. Q.; Hou, Y.; Chai, G. L.; Olianas, D.; Liao, Z. Q.; Milani, A.; Sun, H. J.; Li, W.; Zhang, Z.; Mannsfeld, S.; Zschech, E.; Tommasini, M.; Feng, X. L. Solvent-mediated engineering of copper-metalated acetylenic polymer scaffolds with enhanced photoelectrochemical performance. *J. Mater. Chem. A* **2021**, *9*, 9729−9734.
(36) Basu, M.; Nazir, R.; Mahala, C.; Fageria, P.; Chaudhary, S.; Gangopadhyay, S.; Pande, S. Ag_2S/Ag Heterostructure: A Promising Electrocatalyst for the Hydrogen Evolution Reaction. *Langmuir* **2017**, *33*, 3178−3186.
(37) Maity, P.; Takano, S.; Yamazoe, S.; Wakabayashi, T.; Tsukuda, T. Binding Motif of Terminal Alkynes on Gold Clusters. *J. Am. Chem. Soc.* **2013**, *135*, 9450−9457.
(38) Yang, Z.; Shen, X. Y.; Wang, N.; He, J. J.; Li, X. D.; Wang, X.; Hou, Z. F.; Wang, K.; Gao, J.; Jiu, T. G.; Huang, C. Graphdiyne Containing Atomically Precise N Atoms for Efficient Anchoring of Lithium Ion. *ACS Appl. Mater. Interfaces* **2019**, *11*, 2608−2617.
(39) Huang, W. G.; Wang, X. Z.; Zhang, W. T.; Zhang, S. J.; Tian, Y. X.; Chen, Z. H.; Fang, W. H.; Ma, J. Intraligand charge transfer boosts visible-light-driven generation of singlet oxygen by metal-organic frameworks. *Appl. Catal. B.* **2020**, *273*, No. 119087.
(40) Yao, C. K.; Yuan, A. L.; Wang, Z. S.; Lei, H.; Zhang, L.; Guo, L. M.; Dong, X. P. Amphiphilic two-dimensional graphitic carbon nitride nanosheets for visible-light-driven phase-boundary photocatalysis. *J. Mater. Chem. A* **2019**, *7*, 13071−13079.
(41) McDonald, S. A.; Konstantatos, G.; Zhang, S. G.; Cyr, P. W.; Klem, E. J. D.; Levina, L.; Sargent, E. H. Solution-processed PbS quantum dot infrared photodetectors and photovoltaics. *Nat. Mater.* **2005**, *4*, 138−142.
(42) Wu, S. Q.; Hu, H. Y.; Lin, Y.; Zhang, J. L.; Hu, Y. H. Visible light photocatalytic degradation of tetracycline over TiO_2. *Chem. Eng. J.* **2020**, *382*, No. 122842.
(43) Wu, S. Q.; Li, X. Y.; Tian, Y. Q.; Lin, Y.; Hu, Y. H. Excellent photocatalytic degradation of tetracycline over black anatase-TiO_2 under visible light. *Chem. Eng. J.* **2021**, *406*, No. 126747.
(44) Cao, S. W.; Low, J. X.; Yu, J. G.; Jaroniec, M. Polymeric Photocatalysts Based on Graphitic Carbon Nitride. *Adv. Mater.* **2015**, *27*, 2150−2176.
(45) Liu, J.; Liu, Y.; Liu, N. Y.; Han, Y. Z.; Zhang, X.; Huang, H.; Lifshitz, Y.; Lee, S. T.; Zhong, J.; Kang, Z. H. Metal-free efficient photocatalyst for stable visible water splitting via a two-electron pathway. *Science* **2015**, *347*, 970−974.
(46) Yamakoshi, Y.; Umezawa, N.; Ryu, A.; Arakane, K.; Miyata, N.; Goda, Y.; Masumizu, T.; Nagano, T. Active oxygen species generated from photoexcited fullerene (C_{60}) as potential medicines: $O_2^{-\cdot}$ versus $^1O_2$. *J. Am. Chem. Soc.* **2003**, *125*, 12803−12809.
(47) Goto, H.; Hanada, Y.; Ohno, T.; Matsumura, M. Quantitative analysis of superoxide ion and hydrogen peroxide produced from molecular oxygen on photoirradiated TiO_2 particles. *J. Catal.* **2004**, *225*, 223−229.
(48) Jiang, H. Y.; Zhou, P.; Wang, Y. Y.; Duan, R.; Chen, C. C.; Song, W. J.; Zhao, J. C. Copper-Based Coordination Polymer Nanostructure for Visible Light Photocatalysis. *Adv. Mater.* **2016**, *28*, 9776−9781.
(49) Bader, H.; Sturzenegger, V.; Hoigne, J. Photometric-Method for the Determination of Low Concentrations of Hydrogen-Peroxide by the Peroxidase Catalyzed Oxidation of N,N-Diethyl-P-Phenylenediamine (Dpd). *Water Res.* **1988**, *22*, 1109−1115.
(50) Ghosh, S.; Kouame, N. A.; Ramos, L.; Remita, S.; Dazzi, A.; Deniset-Besseau, A.; Beaunier, P.; Goubard, F.; Aubert, P. H.; Remita, H. Conducting polymer nanostructures for photocatalysis under visible light. *Nat. Mater.* **2015**, *14*, 505−511.
(51) Yin, M. C.; Li, Z. S.; Kou, J. H.; Zou, Z. G. Mechanism Investigation of Visible Light-Induced Degradation in a Heterogeneous TiO_2/Eosin Y/Rhodamine B System. *Environ. Sci. Technol.* **2009**, *43*, 8361−8366.

https://doi.org/10.1021/acsanm.3c00514
ACS Appl. Nano Mater. 2023, 6, 7395−7403